Hindawi
Journal of Chemistry
Volume 2022, Article ID 7844259, 9 pages
https://doi.org/10.1155/2022/7844259

Research Article

Photocatalytic Behavior of Supported Copper Double Salt: The Role of Graphene Oxide

Marjan E. Shabestari, Juan Baselga, and Olga Martin

Department of Materials Science and Engineering and Chemical Engineering, Polytechnic School, Universidad Carlos III de Madrid, Avenida Universidad 30, 28911 Leganés, Madrid, Spain

Correspondence should be addressed to Juan Baselga; jbaselga@ing.uc3m.es

Received 23 November 2021; Revised 22 March 2022; Accepted 8 April 2022; Published 12 May 2022

Academic Editor: Roberto Comparelli

The design of a photocatalyst that may work efficiently with sunlight is a fundamental concern to fight against environmental pollution and electrochemical hydrogen storage devices. In this work, it has been found that the green microwave-assisted decoration of graphene by copper double salt (DS) enhances visible sunlight photocatalysis efficiency. Nanohybrids of graphene oxide decorated with Cu(I) and Cu(II) oxides and copper hydroxy nitrate double salt were selected as photocatalysts for the degradation of rhodamine B in aqueous solution to study the effect of the graphene oxide support. The photodegradation process followed a pseudo–first-order kinetics for the bare catalysts, but the supported catalysts were best fitted to the Langmuir-Hinshelwood model. Supported systems were more efficient in terms of turnover and apparent rate constants. Diffuse reflectance spectroscopy with the use of Kubelka-Munk function allowed to measure bandgap energies. It was found that the absorption edge was reduced about 30% for the supported systems.

1. Introduction

Dyes in wastewater as one of the most important groups of pollutants have a usually recalcitrant nature and are nonbiodegradable. Therefore, a large number of different catalysts and photocatalysts to accelerate the pollutant degradation have been recommended so far today [1–10].

Traditionally, activated carbons with high surface area have been widely used for water purification [11]. Furthermore, graphene, which theoretically shows nearly twice the surface area, can serve as a very good alternative for activated carbon in water purification, but it has not shown promising results in photocatalytic dye degradation [12]. Additionally, graphite and its derivatives (graphene oxide (GO), and reduced graphene oxide (rGO)) have been recognized as attractive catalyst supports because of their significant conductivity, excellent electron mobility, extremely high surface area (~2600 m^2/g), high thermal/electrical conductivity, and chemical stability [13, 14].

On the other hand, metal oxide nanoparticles (MONPs) such as TiO_2, ZnO, SnO_2, MnO_2, Co_3O_4, Fe_3O_4, Fe_2O_3, NiO, and Cu_2O have been employed as photocatalysts to remove dye pollutants from waste water [15]. However, metal oxides present some drawbacks. Firstly, metal oxides are only active in the UV-vis region because of their wide bandgap energy. Secondly, due to the possibility of charge carrier recombination, the lifetime of the active species responsible for the degradation is short [16, 17].

In recent years, the decoration of graphene sheets with metal oxide nanoparticles (MONPs) to prepare graphene metal oxide hybrids has attracted considerable attention for their potential applications in catalysis and photocatalysis fields. The synergetic effect between graphene and MONPs resulted in outstanding properties of graphene hybrids. Graphene oxide as support of photocatalytic metal oxide nanoparticles obtained by green microwave-assisted methods causes interesting effects such as an increase of the specific surface, an increase of catalyst recyclability due to the graphene paramagnetism, a reduction of bandgap energy due to the strong interaction between *d* atomic orbitals and the graphene conjugated system, and stabilization of photoexcited electron-hole pairs suppressing recombination due to

the intrinsic conductivity of graphene, and consequently, oxidative species will be more efficiently created increasing photodegradation performance.

Furthermore, the combination of metal oxides (MO) with electron scavenging agents has been proposed as a strategy to improve the photocatalytic efficiency of MO [18].

Up to now, different methods to synthesize and support MONPs on graphene have been proposed: solution mixing, sol–gel, hydrothermal/solvothermal, self-assembly, microwave, etc. [19].

In this work, we used a convenient microwave-assisted method as an alternative route for the preparation of copper oxide (CuO), cuprous oxide (Cu_2O), and the most important member of copper double salt (DS), copper hydroxy nitrate ($Cu_2(OH)_3(NO_3)$). As already reported [20], the method allowed not only the synthesis of nanoparticles but also the simultaneous decoration of GO. After characterization of the final products by TEM, XRD, Raman, BET, TGA, and UV-vis diffuse reflectance techniques, the performance of the supported and nonsupported nanohybrids as photocatalysts for the degradation reaction of a toxic dye (rhodamine B) in water was studied [21].

2. Experimental Procedures

2.1. Materials. Graphite powder (with a purity > 99.999%) was purchased from Alfa Aesar; H_2O_2 30% *w*/*v* (Panreac), $KMnO_4$ (Panreac), $NaNO_3$ (Sigma-Aldrich), and H_2SO_4 98% *v*/*v* (Panreac) were employed for graphite oxidation and used without any further purification. Copper (II) nitrate hemi(pentahydrate), $Cu(NO_3)_2{\cdot}2.5H_2O$, and rhodamine B (RhB) were purchased from Sigma-Aldrich and Alfa Aesar, respectively.

2.2. Preparation of Copper Nanohybrids/Graphene Oxide. Graphene oxide (GO) was prepared from natural flake graphite powders using a modified Hummers method [22].

Decoration of graphene oxide by copper salts was performed following a new method proposed in our previous work [20]. In brief, for the synthesis of copper hydroxyl nitrate (DS, $Cu_2(OH)_3(NO_3)$, on graphene oxide (DS/GO), a mixture of GO/ethanol (100 mg/50 mL) was dispersed for 5 min under sonication, added to 100 mL 0.01 M $Cu(NO_3)_2$/ethanol solution, and microwaved for 2 minutes. The mixture was filtered after cooling; the precipitate was washed with deionized water and hot ethanol at least for five times and dried in a vacuum oven at 90°C for 12 h.

Decoration of graphene oxide by cuprous oxide (Cu_2O/GO) was performed in the same way as previously but changing the solvent to ethylene glycol.

Heating of DS/GO at 250°C for 10 min in an oven led up to graphene oxide decorated by copper oxide (CuO/GO). Nonsupported DS, Cu_2O, and CuO were synthesized also using the same procedures but in the absence of graphene oxide to compare the performance of supported and nonsupported copper nanoparticles.

2.3. Characterization of Nanoparticles. Characterization of the synthesized nanohybrids was performed by XRD, TGA, TEM, Raman, FTIR, and specific surface measurements, BET, as previously reported [20]. Results clearly showed a good anchoring of the copper compound nanoparticles on the surface of exfoliated graphene oxide nanosheets.

Bandgap energy determinations were performed through diffuse reflectance spectrum (DRS) measurements of all samples with a Lambda 14P, Perkin-Elmer spectrophotometer in the diffuse reflectance mode $F(R_\infty)$ (absolute reflectance), using a 60 mm integration sphere and $BaSO_4$ as pattern.

2.4. Photocatalytic Test. Photocatalysis tests were performed studying the decomposition kinetics of a well-known dye such as rhodamine B (RhB) in aqueous solution under ambient dark conditions. RhB was selected as a model compound because it is a toxic colorant commonly used in textile industries although it is highly stable under native light; it is toxic, nonbiodegradable, and nondegradable in the absence of any photocatalyst [23, 24]. The experimental setup is schematically depicted in Figure 1. The reaction chamber was optically isolated to avoid undesired effects due to ambient light and to prevent leakage of harmful UV light. It was also thermally isolated by a water jacket to avoid thermal effects from the UV source (TQ 150 W). All experiments were done at room temperature.

In a typical experiment, 10 mg of the synthesized catalyst was dispersed in 100 mL of water and sonicated for 5 min. The suspension was added to 400 mL of RhB stock solution to achieve a RhB concentration around 10 mg·L^{-1}. Before starting irradiation, the suspension was stirred moderately in darkness for 30 minutes to ensure the adsorption/desorption equilibrium of the organic dye. Then UV-vis light was switched on. Approximately 2 mL of the suspension was removed from the photodegradation chamber at fixed intervals (30 minutes), and RhB concentration was measured by spectrophotometry (Jasco V-650). Linearity between absorbance at 554 nm and RhB concentration was previously checked in the range 1 to 10 ppm. Complementary tests to check the light effect in the absence of any catalyst as well as the effect of GO in the absence of illumination were also performed.

3. Results and Discussion

A summary of the main characterization data from our previous work [20] is presented in Table 1. Adsorption isotherms and pore size are presented as supplementary information in Figure S1. The microwave-based synthesis method yielded GO sheets fully covered with particles (DS, Cu_2O, and CuO), with weight fractions ranging between 76 and 97%, probably because the functional groups of GO (carbonyl, epoxy, and hydroxyl groups) act as the nucleation sites for the growth of nanoparticles [25]. The size of the crystallites as measured by the Scherrer equation was similar for bare and supported particles. However, the most relevant result was the notable difference in surface area: the supported particles present a higher surface than unsupported samples.

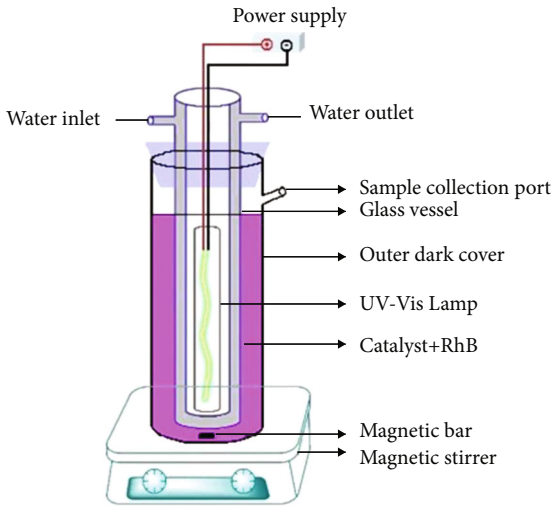

Figure 1: Experimental setup for photodegradation of RhB.

Table 1: Calculated average crystallite size (Scherrer), surface area, and % (w/w) of Cu compound in the catalyst of supported and nonsupported nanoparticles in GO.

	Crystallite size (nm)		Surface area (m^2/g)		% (w/w) Cu
	Supported	Unsupported	Supported	Unsupported	
Cu_2O	9	9	102	74	75.8
DS	27	47	142	1.6	88.6
CuO	18	21	209	1.5	96.7
GO	—	—	1132	—	—

3.1. Photodegradation Performance of Catalysts. Photodegradation experiments were done in the presence of GO, DS/GO, Cu_2O/GO, CuO/GO, and bare DS, Cu2O, and CuO to study the effect of GO as substrate. In addition, the performance of TiO_2 Degussa P-25 as a common photocatalyst reference [26] was also tested for comparison purposes.

At several irradiation times, UV-vis spectra of the reaction mixture were recorded. As an example, Figure 2 depicts the absorbance spectra of the remaining RhB for tests in which DS and DS/GO were used as photocatalysts. Other catalysts showed similar trends. The main absorption peak of RhB at 554 nm decreases with time as the degradation proceeds, and the comparison of both figures clearly shows that the rate of degradation with supported catalyst is higher than that with the bare salt.

In addition, no shift in the absorption maxima was detected for any of the studied catalysts (bare or supported particles), reflecting that the degradation products do not absorb light and this suggests that RhB mineralization is the main photodegradation pathway [27]. Photodegradation conversion was defined as $\alpha = 100 \times (C_0 - C_t)/C_0$, where C_0 and C_t are the concentrations of RhB at start and at time t. A plot of α against photodegradation time is presented in Figure 3.

This figure shows that (i) the decomposition of RhB under irradiation without any catalyst (<5% during 240 min exposure) is negligible; (ii) the kinetic profiles of systems containing GO with and without irradiation are almost equal within the experimental error, suggesting that GO catalytic activity is not negligible although small and independent of irradiation; (iii) each of the bare nanoparticles Cu_2O, CuO, and DS catalyzes photodegradation with apparently different kinetics but is much more less active than supported catalysts; (iv) the reference catalyst (TiO_2) is more effective than bare nanoparticles but much less active than supported nanohybrids; and (v) all supported catalysts are able to reduce RhB concentration in more than 90% in less than 240 min under the irradiation conditions used in this work.

These experiments confirm the superior photocatalytic activity of the supported catalysts; however, it should be pointed out that no significant differences in catalytic activity were apparently found for the supported systems, contrary to what is observed for the bare nanoparticles. In addition, in our previous study on the catalytic activity of GO-supported systems in several chemical reactions (oxidation, C-C, C-N, and C-S coupling reactions) [20], significant differences were found between them, especially for copper hydroxide nitrate (DS), which presented an outstanding turnover number (TON) in all studied reactions. Therefore, now, two questions may arise: (i) why do GO-supported systems present higher activity than nonsupported ones? And (ii) why is there no difference in the photocatalytic activity of the supported systems while there is in coupling reactions?

To answer these questions, we tried to analyze the data in terms of some kinetic models and a detailed study of the bandgap energy of the GO-supported systems.

3.2. Photocatalytic Degradation Kinetics. Rhodamine usually follows pseudo–first-order photodegradation kinetics in the presence of nonsupported heterogeneous catalysts (Equation (1)) [28].

$$C = C_0 e^{-k_{app} t}, \quad (1)$$

where k_{app} is the apparent first-order reaction rate. For fitting purposes, this equation was linearized in terms of the conversion and it was allowed free intercept.

$$\ln \frac{C_0}{C_t} = \ln (1 - \alpha) = k_{app} t. \quad (2)$$

In Figure 4, we present the plot of $\ln (1 - \alpha)$ versus time for all the unsupported systems. Linear fits confirm that nonsupported systems followed this simple kinetic model, although attempts to fit kinetic data for GO-supported systems failed.

Apparent rate constants and correlation coefficients for the bare particles and GO are presented in Table 2.

Kinetic data for supported systems was analyzed in terms of the Langmuir-Hinshelwood model for heterogeneous catalytic unimolecular reactions [29]. This model assumes an adsorption/desorption equilibrium of the dye and degradation by-products over the catalyst and, once

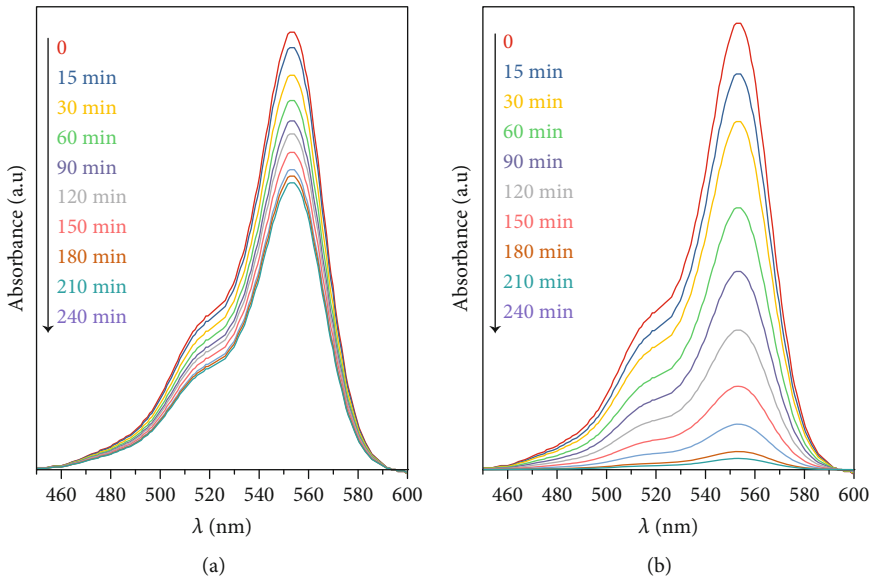

Figure 2: Absorbed light spectra for RhB at different reaction times affected by (a) DS and (b) DS/GO catalysts.

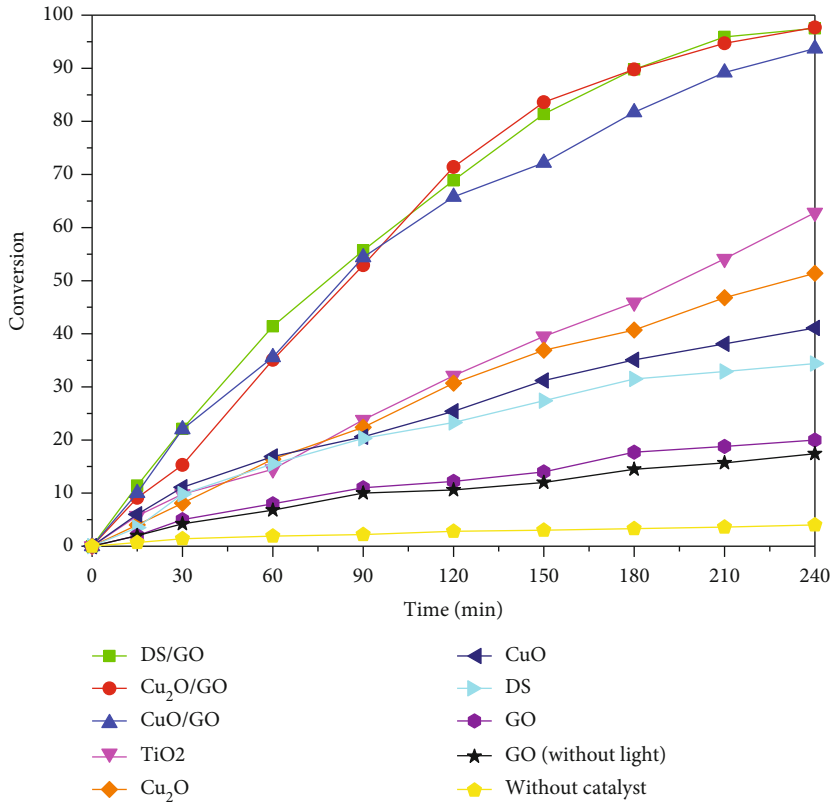

Figure 3: Photodegradation conversion of RhB as a function of irradiation time in the presence of different catalysts.

the dye is adsorbed, a slow unimolecular degradation step. The typical rate equation for this model is given in the following equation:

$$r = -\frac{dC}{dt} = \frac{k_r K C_t}{1 + K C_t}, \quad (3)$$

where r represents the reaction rate, K is the equilibrium constant for the adsorption of the substrate on GO, and k_r is the limiting rate constant of the reaction at the maximum coverage of the solid support. The product $k_r K$ is sometimes globally evaluated as an apparent rate constant (k_{app} ; min^{-1}) and can be compared with the rate constants of bare

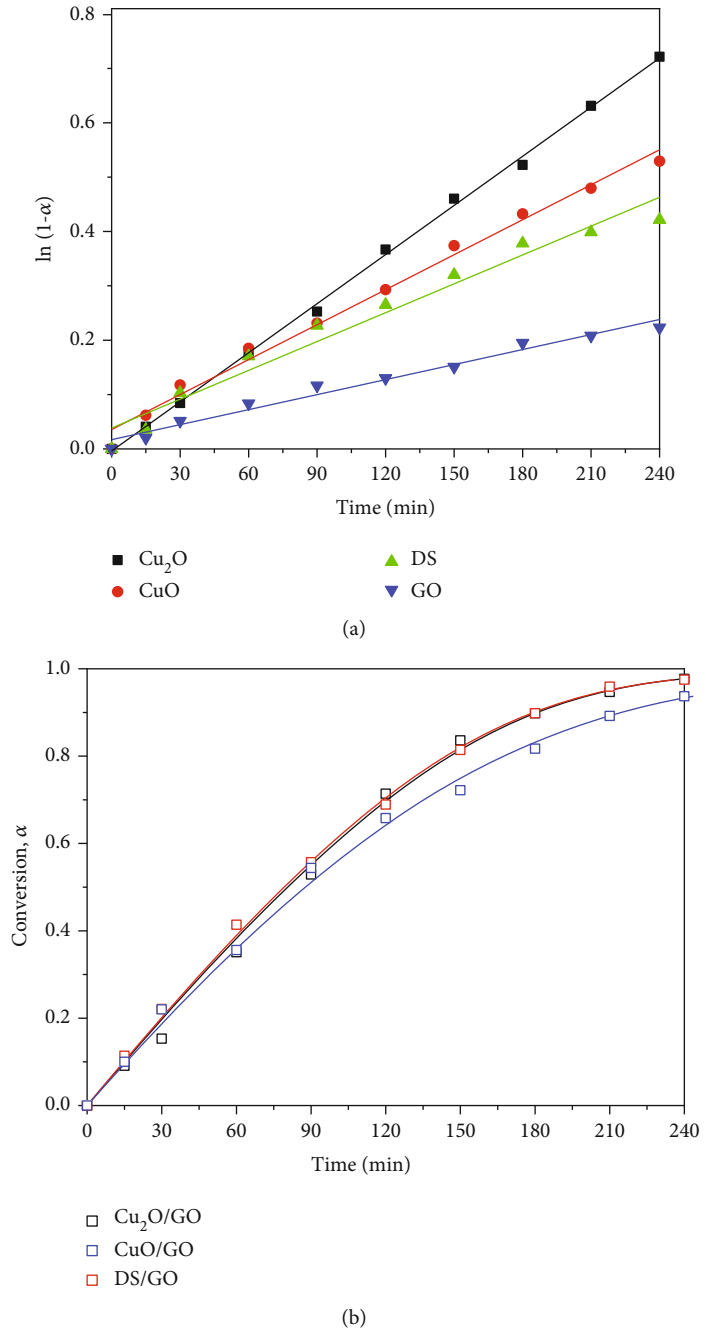

FIGURE 4: (a) $\ln(1-\alpha)$ vs. time for unsupported catalysts and GO systems. (b) Conversion vs. time plots for three supported catalyst systems.

particles. The integrated form of Equation (3) is [30]

$$\frac{C}{C_0} = e^{K(C_0-C)}e^{-k_rKt}. \quad (4)$$

Equation (4) can be expressed linearly in terms of the conversion degree in a nonexponential form as follows:

$$KC_0\alpha - \ln(1-\alpha) = k_rKt. \quad (5)$$

Linear fitting of Equation (5) allows finding the constants $k_{app} = k_rK$ and K, which are also presented in Table 2.

According to Wachs et al. [31], one of the interesting parameters to compare heterogeneous photocatalysis activity is the turnover rate (TOR, defined as moles converted or produced per gram of photocatalyst per unit of time). Results for TOR are also given in Table 2.

Experimental conversion vs. time plots are presented in Figure 4(b). Fitting lines for the supported systems show an excellent agreement with the L-H model.

Table 2: Calculated rate constants for all studied systems.

System	k_{app} (min^{-1})	K (L/mg)	$TOR * \times 10^7$ (mol/g·min)	r^2
Cu_2O	$(3.01 \pm 0.04) \cdot 10^{-3}$	—	2.3	0.999
DS	$(1.77 \pm 0.11) \cdot 10^{-3}$	—	2.1	0.96
CuO	$(2.14 \pm 0.08) \cdot 10^{-3}$	—	2.5	0.988
GO	$(0.92 \pm 0.05) \cdot 10^{-3}$	—	1.3	0.97
Cu_2O/GO	$(2.94 \pm 0.62) \cdot 10^{-2\#}$	0.83 ± 0.12	4.54	0.997
DS/GO	$(2.86 \pm 0.48) \cdot 10^{-2\#}$	0.77 ± 0.09	5.25	0.998
CuO/GO	$(1.85 \pm 0.58) \cdot 10^{-2\#}$	0.46 ± 0.09	4.91	0.996

TOR∗: turnover rate. #Apparent rate constant from the Langmuir-Hinshelwood model.

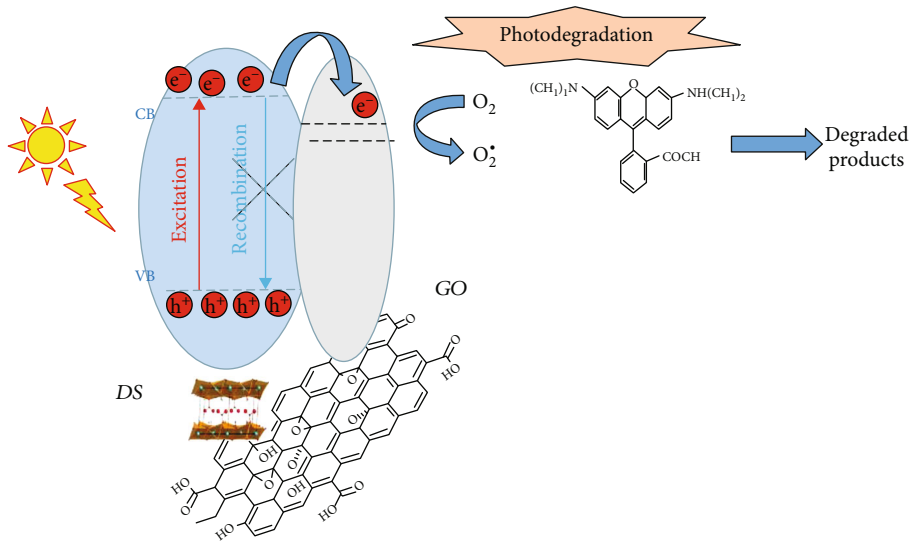

Figure 5: Schematic illustration of band levels and charge transfer in GO-DS nanoparticles.

The rate constants are in the range of 10^{-3} min^{-1} for the bare particles while the apparent rate constant for the GO-supported systems is one order of magnitude higher. As a consequence, the activity of the supported catalysts, as indicated by TOR data, approximately doubles that of the bare particles. However, considering the standard deviation of the fitting parameters, there appear to be significant differences in the rate constant among the bare particles, but those differences disappear for the supported systems, i.e., the latter present almost the same apparent rate constant $\langle k_{app} \rangle = 2.55 \pm 0.56\,min^{-1}$. This fact must be undoubtedly attributed to the presence of GO; i.e., the effect of GO as a support is more important than the nature of the decorating particle on the kinetics of photodegradation at least, for the studied systems.

Data on K, the adsorption/desorption equilibrium constant, reveal that GO provides its surface for the adsorption of the dye and if adsorption plays a fundamental role, K should correlate with specific surface values of the supported catalysts. Recalling the specific surface data appearing in Table 1 and N_2 adsorption/desorption curves of supported catalysts (Fig S1 c), we can observe that specific surface varies in the range of 100-200 m^2/g for the supported systems, higher than for the bare particles, but it seems that there is no correlation between the available surface for dye adsorption and the value of K, or even with k_{app}. This means that the relevant effect of GO must not be related to its surface but probably to its influence on the electronic mechanism of dye photodegradation.

3.3. Bandgap Energy. The common mechanism of heterogeneous photocatalysis with semiconductors involves the excitation of valence band electrons to the conduction band of the catalyst by irradiation with an appropriate wavelength creating thus an electron-hole pair, Figure 5. The produced electrons and holes interact with oxygen and water forming various reactive oxidative species able to oxidize RhB by a collection of specific redox reactions [32, 33] which typically involve hydroxyl radicals.

According to the literature, graphene oxide as a semiconducting support should have the following effects on this mechanism: (i) the extended π conjugation structure allows a strong interaction with metal oxide particles through the overlap with atomic d orbitals and facilitates the catalyst-support electron transfer process [34], (ii) this interaction should shift the valence band edge and reduce the bandgap

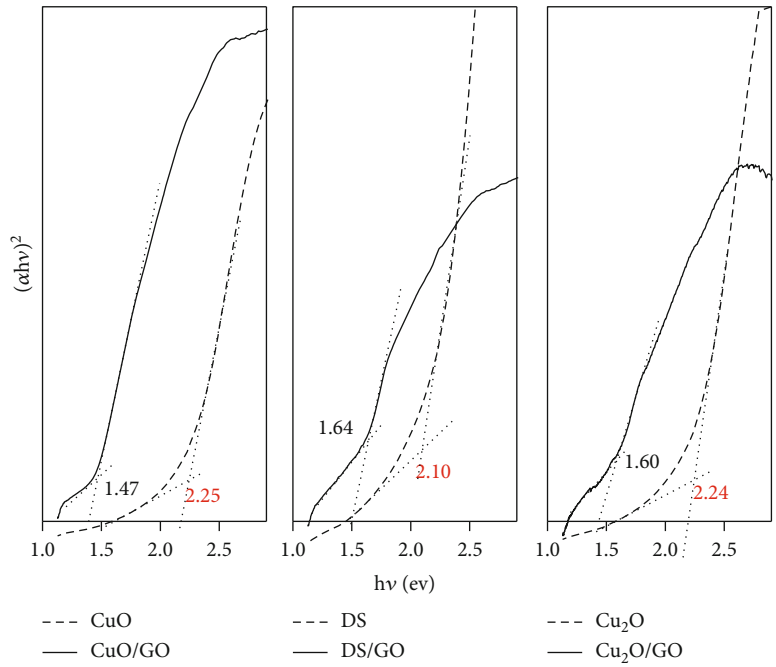

Figure 6: Bandgap from the Kubelka-Munk transformed reflectance spectra for all catalysts.

Table 3: Bandgap energy extracted from Figure 5.

Catalyst	Bandgap energy (ev)	
	Unsupported	Supported
Cu_2O	2.24	1.60
DS	2.10	1.64
CuO	2.25	1.47

Table 4: Bibliographic experimental data for rhodamine B photodegradation.

Photocatalyst particles	Photoc. efficiency (%)	Irradiation time (min)	Ref.
In_2S_3/In-MOF	92.2	120	[38]
TiO_2	25	40	[29]
ZnO	89	120	[30]
TiO_2	99.1	120	[31]
P-nLi_2SnO_3/g-C_3N_4	86	60	[32]
rGO/ZnO	98.78	120	[33]
rGO/TiO_2	99	60	[34]
ZnO/SiO_2	99	240	[35]
$SnO_2/SiO_2 + NaBH_4$	99.9	5	[36]
ZrO_2/SiO_2	99.99	60 min	[37]

of copper salts extending the wavelength absorption range [35]; and (iii) the GO conductivity hinders electron-hole recombination from catalyst producing more efficiently the highly oxidizing species. Consequently, a more active catalyst should be obtained.

To confirm the effect of GO on the bandgap of the catalyst, diffuse reflectance spectroscopy was utilized. Optical bandgaps could be estimated from Tauc plots [36] as presented in Figure 6 and Table 3. This analysis revealed that the absorption edge of the supported catalysts was red shifted and the bandgaps were 22–35% smaller than the corresponding bare salts. Differences among them can be attributed to the crystalline size/morphology and type of electronic transition due to the covalent link between copper salts and graphene oxide [37, 22]. These results confirm thus the mechanism by which GO as a support increases the overall efficiency of the studied catalysts and facilitates the catalysts to be used under safer sunlight-like conditions. Results found for similar systems in the recent literature (Table 4) [38–47] show that the systems studied in this work show similar photocatalytic efficiency.

4. Conclusions

The role of graphene oxide as a catalyst support has been analyzed in the photocatalytic degradation reaction of a common dye, rhodamine B. The selected catalysts were Cu (I) and Cu(II) oxides as well as copper hydroxy nitrate double salt. Bare and supported catalysts were obtained via a green microwave-assisted method, as reported in our previous work [20].

Kinetics of the photocatalytic degradation of rhodamine B was followed for both the bare and the supported catalytic systems. Results for the double salt were reported for the first time. It was found that the supported systems are more efficient catalysts as revealed by their higher apparent reaction rate and higher turnover. Analysis of the apparent rate constants and of the adsorption/desorption equilibrium constant revealed that the effect of GO as a support (i) is more important than the nature of the decorating catalyst and

(ii) must not be related to its surface but to its influence on the electronic mechanism of dye photodegradation.

Bandgaps were measured for the studied systems through diffuse reflectance spectroscopy. For the supported systems, it was found that the light absorption edge becomes redshifted, and the bandgaps were 22–35% smaller than the corresponding energy gaps for the bare salts. Therefore, copper-based catalysts supported by GO are more efficient because (i) the excellent electron mobility of GO facilitates charge separation and stabilization of photoexcited electron-hole pairs suppressing their recombination and (ii) increases the efficiency of light collection towards a safer sunlight-like wavelength range.

Data Availability

Data are available on request.

Conflicts of Interest

The authors declare that they have no known competing financial interests or personal relationships that could have appeared to influence the work reported in this paper.

Authors' Contributions

Marjan E. Shabestari was responsible for the synthesis of Cu GO-supported and unsupported nanoparticles, photocatalysis experiments, and writing a paper draft. Olga Martin was responsible for advice in synthesis of particles and interpretation of characterization. Juan Baselga was responsible for advice on characterization and correction of draft paper.

Acknowledgments

The authors wish to thank Ministerio de Ciencia, Innovación y Universidades grant MAT2014-57557-R. Additionally, the authors would like to thank to Diogo Videira-Quintela for the invaluable help in the characterization of samples.

Supplementary Materials

Figure S1: (a) BET results of N_2 adsorption/desorption isotherms of supported catalyst. (b) Adsorption isotherms of bare catalyst. (c) Adsorption isotherms of supported catalyst. (d) Pore diameter of bare and supported catalyst. *(Supplementary Materials)*

References

[1] M. Amir, A. Jahangeer, M. A. Saad, M. Yuanbing, and A. Tokeer, "rare earth doped metal oxide nanoparticles for photocatalysis: a perspective," *Nanotechnology*, vol. 33, no. 14, article 142001, 2022.

[2] S. Zinatloo-Ajabshira, M. Sadat Morassaeib, O. Amiric, and M. Salavati-Niasari, "Green synthesis of dysprosium stannate nanoparticles using Ficus carica extract as photocatalyst for the degradation of organic pollutants under visible irradiation," *Ceramic International*, vol. 46, pp. 6095–6107, 2020.

[3] R. Monsef, M. Ghiyasiyan-Arani, and M. Salavati-Niasar, "Design of magnetically recyclable ternary Fe2O3/EuVO4/g-C3N4Nanocomposites for photocatalytic and electrochemical hydrogen storage," *ACS Applied Energy Materials*, vol. 4, no. 1, pp. 680–695, 2021.

[4] M. Salavati-Niasari, D. Ghanbari, and F. Davar, "Synthesis of different morphologies of bismuth sulfide nanostructures via hydrothermal process in the presence of thioglycolic acid," *Journal of Alloys and Compounds*, vol. 488, no. 1, pp. 442–447, 2009.

[5] R. B. P. Marcelino and C. C. Amorim, "Towards visible light photocatalysis for environmental applications: band-gap engineering versus photons absorption-a review," *Environmental Science and Pollution Research*, vol. 26, no. 5, pp. 4155–4170, 2019.

[6] J. He, A. Meng, B. Cheng, W. Ho, and J. Yu, "Enhanced photocatalytic H_2-production activity of WO_3/TiO_2 step-scheme heterojunction by graphene modification," *Journal of Catalysis*, vol. 41, no. 1, pp. 9–20, 2020.

[7] Q. Li, W. Zhao, Z. Zhai et al., "2D/2D Bi_2MoO_6/g-C_3N_4 S-scheme heterojunction photocatalyst with enhanced visible-light activity by Au loading," *Journal of Materials Science and Technology*, vol. 56, pp. 216–226, 2020.

[8] Z. Li, Z. Wu, R. He, L. Wan, and S. Zhang, "$In_2O_{3-x}(OH)_y$ /Bi_2MoO_6 S-scheme heterojunction for enhanced photocatalytic performance," *Journal of Materials Science and Technology*, vol. 56, pp. 151–161, 2020.

[9] L. Zhang, S. Zhao, X. Cheng, Z. Liu, R. Liu, and G. Dawson, "Enhaced photocatalytic activity of Brown $H_4Nb_6O_{17}$/g-C_3N_4 composite for visible-light driven H_2O_2 production," *Chemical Engineering Journal*, vol. 429, article 132587, 2022.

[10] S. Gaikwad, N. Jadhav, S. Mahadik, A. G. Thoka, and M. B. Mandake, "Review: photocatalytic degradation of textile azo dyes," *International Journal of Advance Engineering and Research Development*, vol. 4, pp. 88–91, 2017.

[11] T. Razvigorova, N. Budinova, N. Petrov, and V. Minkova, "Purification of water by activated carbons from apricot stones, lignites and anthracite," *Water Research*, vol. 32, no. 7, pp. 2135–2139, 1998.

[12] J. McAllister, J. L. Li, D. H. Adamson et al., "Single sheet functionalized graphene by oxidation and thermal expansion of graphite," *Chemistry of Materials*, vol. 19, no. 18, pp. 4396–4404, 2007.

[13] B. Gawande, A. Goswami, F. X. Felpin et al., "Cu and Cu-based nanoparticles: synthesis and applications in catalysis," *Chemical Reviews*, vol. 116, no. 6, pp. 3722–3811, 2016.

[14] K. Dhand, Y. Rhee, H. J. Kim, and D. H. Jung, "A comprehensive review of graphene nanocomposites: research status and trends," *Journal of Nanomaterials*, vol. 2013, 763914 pages, 2013.

[15] W. Lin, L. Jiang, P. Chen, H. W. Xu, and H. Wang, "Treatment of produced water with photocatalysis: recent advances, affecting factors and future research prospects," *Catalysts*, vol. 10, no. 8, p. 924, 2020.

[16] S. Chatterjee and S. Dasgupta, "Visible light induced photocatalytic degradation of organic pollutants," *Journal of Photochemistry and Photobiology C*, vol. 6, no. 2-3, pp. 186–205, 2005.

[17] V. S. Arora, K. Jaswal, R. Singh, and R. Singh, "Applications of metal/mixed metal oxides as photocatalyst: a review," *Oriental Journal of Chemistry*, vol. 32, no. 4, pp. 2035–2042, 2016.

[18] F. Ruffino and F. Giannazzo, "A review on metal nanoparticles nucleation and growth on/in graphene," *Crystals*, vol. 7, no. 7, pp. 219–258, 2017.

[19] T. Hu, F. Lu, R. Chen, and R. Zhang, "A brief review of graphene–metal oxide composites synthesis and applications in photocatalysis," *Journal of the Chinese Advanced Materials Society*, vol. 1, no. 1, pp. 21–39, 2013.

[20] O. Shabestari, D. Martín, S. Díaz-García, V. J. Gómez-Ruiz, J. Gonzalez, and J. Baselga, "Facile and rapid decoration of graphene oxide with copper double salt, oxides and metallic copper as catalysts in oxidation and coupling reactions," *Carbon*, vol. 161, pp. 7–16, 2020.

[21] M. Shabestari, *Doping & Decoration of Carbon based Nanoparticles: Applications in Flame Retardancy and Catalysis, [Ph.D. thesis]*, Universidad Carlos III de Madrid, 2019.

[22] S. Hummers and R. E. Offeman, "Preparation of graphitic oxide," *Journal of the American Chemical Society*, vol. 80, no. 6, p. 1339, 1958.

[23] J. Kornprobst and J. Plank, "Photodegradation of rhodamine b in presence of CaO and NiO-CaO catalysts," *International Journal of Photoenergy*, vol. 2012, 6 pages, 2012.

[24] T. Soares, M. A. Lansarin, and C. C. Moro, "A study of process variables for the photocatalytic degradation of rhodamine B," *Brazilian Journal of Chemical Engineering*, vol. 24, no. 1, pp. 29–36, 2007.

[25] H. Hao, L. Song, X. Zhang, Y. Wan, Y. Tang, and Y. Lv, "SiO_2/graphene composite for highly selective adsorption of Pb(II) ion," *Journal of Colloid and Interface Science*, vol. 369, no. 1, pp. 381–387, 2012.

[26] M. Mahlambi, C. J. Ngila, and B. B. Mamba, "Recent developments in environmental photocatalytic degradation of organic pollutants: the case of titanium dioxide nanoparticles—a review," *Journal of Nanomaterials*, vol. 2015, Article ID 790173, 29 pages, 2015.

[27] S. Zhang, M. Zhai, H. Wang et al., "Photocatalytic degradation of rhodamine B by using a nanocomposite of cuprous oxide, three-dimensional reduced graphene oxide, and nanochitosan prepared via one-pot synthesis," *Journal of Alloys and Compounds*, vol. 659, pp. 101–111, 2016.

[28] R. Yu, Z. Cai, and Z. Liu, "Studies on the photodegradation of rhodamine dyes on nanometer-sized zinc oxide," *Spectrochimica Acta Part A*, vol. 60, no. 7, pp. 1617–1624, 2004.

[29] D. Xu and H. Ma, "Degradation of rhodamine B in water by ultrasound-assisted TiO_2 photocatalysis," *Journal of Cleaner Production*, vol. 313, article 127758, 2021.

[30] T. M. O. Ruellas, G. H. S. Domingos, L. O. O. Peçanha, S. C. Maestrelli, and T. R. Giraldi, "Photodegradation of rhodamine B catalyzed by ZnO pellets," *Cerâmica*, vol. 65, Supplement 1, pp. 47–53, 2019.

[31] Z. Liu, Z. W. Li, Z. Q. Wu, and X. H. Xia, "Study on the photocatalytic reaction kinetics in a TiO_2 nanoparticles coated microreactor integrated microfluidics device," *Talanta*, vol. 182, pp. 544–548, 2018.

[32] Y. Li, M. Wu, Y. Wang et al., "Novel P-n Li_2SnO_3/g-C_3N_4 heterojunction with enhanced visible light photocatalytic efficiency toward rhodamine B degradation," *Frontiers in Chemistry*, vol. 8, p. 75, 2020.

[33] S. Ramanathan, S. P. Selvin, A. Obadiah et al., "Synthesis of reduced graphene oxide/ZnO nanocomposites using grape fruit extract and *Eichhornia crassipes* leaf extract and a comparative study of their photocatalytic property in degrading rhodamine B dye," *Journal of Environmental Health Science and Engineering*, vol. 17, no. 1, pp. 195–207, 2019.

[34] M. S. Adly, S. M. El-Dafrawy, and S. A. El-Hakam, "Application of nanostructured graphene oxide/titanium dioxide composites for photocatalytic degradation of rhodamine B and acid green 25 dyes," *Journal of Materials Research and Technology*, vol. 8, no. 6, pp. 5610–5622, 2019.

[35] X. Shen, Y. Shi, H. Shao, Y. Liu, and Y. Zhai, "Synthesis and photocatalytic degradation ability evaluation for rhodamine B of ZnO@ SiO_2 composite with flower-like structure," *Water Science and Technology*, vol. 80, no. 10, pp. 1986–1995, 2019.

[36] S. M. A. Francis and V. Thiruvengadam, "Catalytic reduction of rhodamine B and crystal violet using SnO_2–SiO_2 nanocomposite derived from rice husk," *International Research Journal of Engineering and Technology*, vol. 7, pp. 2094–2097, 2020.

[37] D. S. S. Padovini, A. G. Magdalena, R. G. Capeli et al., "Synthesis and characterization of ZrO_2@SiO_2 core-shell nanostructure as nanocatalyst: application for environmental remediation of rhodamine B dye aqueous solution," *Materials Chemistry and Physics*, vol. 233, pp. 1–8, 2019.

[38] L. Hu, D. Mao, L. Yang et al., "In_2S_3 nanoparticles coupled to In- MOF nanorods: the structural and electronic modulation for synergetic photocatalytic degradation of rhodamine B," *Environmental Research*, vol. 203, article 111874, 2022.

[39] E. Davis and R. J. Davis, *Fundamentals of Chemical Reaction Engineering, Chapter 5: Heterogeneous Catalysis*, McGraw Hill, New York, NY, USA, 2003.

[40] G. Asenjo, R. Santamaría, C. Blanco, M. Granda, P. Álvarez, and R. Menéndez, "Correct use of the Langmuir-Hinshelwood equation for proving the absence of a synergy effect in the photocatalytic degradation of phenol on a suspended mixture of titania and activated carbon," *Carbon*, vol. 55, pp. 62–69, 2013.

[41] S. P. Wachs, C. A. Phivilay, and C. A. Roberts, "Reporting of reactivity for heterogeneous photocatalysis," *ACS Catalysis*, vol. 3, no. 11, pp. 2606–2611, 2013.

[42] A. A. Isari, A. Payan, M. Fattahi, S. Jorfi, and B. Kakavandi, "Photocatalytic degradation of rhodamine B and real textile wastewater using Fe-doped TiO_2 anchored on reduced graphene oxide (Fe-TiO_2/rGO): characterization and feasibility, mechanism and pathway studies," *Applied Surface Science*, vol. 462, pp. 549–564, 2018.

[43] B. Viswanathan, "Photocatalytic degradation of dyes: an overview," *Current Catalysis*, vol. 7, no. 2, pp. 99–121, 2018.

[44] D. Albero, H. Mateo, and H. García, "Graphene-based materials as efficient photocatalysts for water splitting," *Molecules*, vol. 24, no. 5, p. 906, 2019.

[45] J. Yeh, C. Cihlář, C. Chang, H. Cheng, and H. Teng, "Roles of graphene oxide in photocatalytic water splitting," *Materials Today*, vol. 16, no. 3, pp. 78–84, 2013.

[46] M. Makuła, W. Pacia, and W. Macyk, "How to correctly determine the band gap energy of modified semiconductor photocatalysts based on UV–Vis spectra," *Journal of Physical Chemistry Letters*, vol. 9, no. 23, pp. 6814–6817, 2018.

[47] J. L. Li and T. Zeng, "A facile synthesis of CuO nanowires and nanorods, and their catalytic activity in the oxidative degradation of rhodamine B with hydrogen peroxide," *Catalysis Communications*, vol. 46, pp. 169–173, 2014.